Journal of Materials Chemistry C

Broadband Light Emitting Zero-Dimensional Antimony and Bismuth-Based Hybrid Halides with Diverse Structures

Journal:	*Journal of Materials Chemistry C*
Manuscript ID	TC-ART-09-2021-004198.R1
Article Type:	Paper
Date Submitted by the Author:	18-Oct-2021
Complete List of Authors:	Deng, Chenkai; University of Science and Technology Beijing Hao, Shiqiang; Northwestern University, Materials Science Liu, Kunjie; University of Science and Technology Beijing Molokeev, Maxim; Kirensky Institute of Physics SB RAS, Wolverton, Chris; Northwestern University, Department of Materials Science and Engineering Fan, Liubing; University of Science and Technology Beijing Zhou, Guojun; Shanxi Normal University, School of Chemistry and Material Science Chen, Da; University of Science and Technology Beijing, Zhao, Jing; University of Science and Technology Beijing, School of Materials Science and Engineering Liu, Quanlin; University of Science and Technology Beijing, School of Materials science & engineering

Journal Name

ARTICLE

Broadband Light Emitting Zero-Dimensional Antimony and Bismuth-Based Hybrid Halides with Diverse Structures

Received 00th January 20xx,
Accepted 00th January 20xx

DOI: 10.1039/x0xx00000x

Chenkai Deng†, Shiqiang Hao‡, Kunjie Liu†, Maxim S. Molokeev ⊥ , Christopher Wolverton‡, Liubing Fan†, Guojun Zhou Δ, Da Chen†, Jing Zhao†,*, Quanlin Liu†,*

Low-dimensional organic–inorganic metal halides have recently attracted extensive attention because of their various structures and distinguished photoelectric properties. Herein, we report a series of new zero-dimensional organic–inorganic hybrid metal halides: $(TMEDA)_3Bi_2Cl_{12}\cdot H_2O$, $(TMEDA)_3Bi_2Br_{12}\cdot H_2O$, $(TMEDA)_3Sb_2Br_{12}\cdot H_2O$, and $(TMEDA)_5Sb_6Cl_{28}\cdot 2H_2O$ [TMEDA = N, N, N′·trimethylethylenediamine]. $(TMEDA)_3M_2X_{12}\cdot H_2O$ (*M* = Bi or Sb, *X* = Cl or Br) crystallizes in the monoclinic space group $P2_1/n$, and $(TMEDA)_5Sb_6Cl_{28}\cdot 2H_2O$ crystallizes in the orthorhombic space group *Pnma*. $(TMEDA)_3M_2X_{12}$ possesses a zero-dimensional structure with the metal halide ions of $[MBr_6]^{3-}$ isolated by the organic $TMEDA^{2+}$ cations. Interestingly, the $(TMEDA)_5Sb_6Cl_{28}\cdot 2H_2O$ structure consists of a combination of corner-connected octahedra $[Sb_4Cl_{18}]^{6-}$ and edge-shared $[Sb_2Cl_{10}]^{4-}$, which is quite rare. The light emission of all these compounds were measured, and $(TMEDA)_3Sb_2Br_{12}\cdot H_2O$ exhibits the most intense luminescence. Upon 400 nm ultraviolet light excitation, $(TMEDA)_3Sb_2Br_{12}\cdot H_2O$ exhibited strong broadband yellow emission centered at 625 nm with a full-width at half-maximum of ~150 nm originating from self-trapped exciton. This work suggests the possibility of new types of hybrid halides by introducing different metal centers and probing the structural evolution and photoluminescent properties, serving as a reference for the relationship between structure and luminescent performance and demonstrating their potential use as phosphors in light-emitting diodes.

1. Introduction

stablishing a framework with functional units and the rational design of new organic–inorganic metal halides (OIMHs) will enable the expansion of the database of emerging materials, especially as they will contribute to different optoelectronic applications, including photodetectors,[1] solar cells,[2-3] and light-emitting diodes (LEDs).[4-5] The wide variety of available organic ligands make these metal halides highly tunable, enabling the synthesis of three-, two-, one-, and zero-dimensional compounds that can easily form single crystals, nanocrystals, and thin-film materials.[6-9] Among them, zero-dimensional (0D) OIMHs exhibit excellent photoluminescent (PL) emissions derived from self-trapped excitons due to strong quantum confinement effects and have become star materials with unprecedented optoelectronic properties.[10-14] Furthermore, the photophysical properties of zero-dimensional OIMHs show high structural adjustability, achieved by engineering the chemical composition and dimensionality as well as the structural distortion degrees. Hence, it remains challenging to understand this type of material and improve the PL properties based on structural analysis.

Low-dimensional OIMHs belong to one type of unique system with tunable photoluminescent properties derived from the synergistic contributions of their organic and inorganic

† *The Beijing Municipal Key Laboratory of New Energy Materials and Technologies, School of Materials Sciences and Engineering, University of Science and Technology Beijing, Beijing 100083, China.*
‡ *Department of Materials Science and Engineering, Northwestern University, Evanston, Illinois 60208, United States.*
⊥ *Laboratory of Crystal Physics, Kirensky Institute of Physics, Federal Research Center KSC SB RAS, Krasnoyarsk 660036 (Russia), Siberian Federal University, Krasnoyarsk, 660041 (Russia) Department of Physics, Far Eastern State Transport University Khabarovsk, 680021 (Russia)*
Δ *Key Laboratory of Magnetic Molecules and Magnetic Information Materials (Ministry of Education), School of Chemistry and Material Science, Shanxi Normal University, Linfen 041004, China*

constituents. On the one hand, the spatial stereoscopic effects of organic cations play a critical role in modifying the anionic structural types and distortion degrees of [MX_6] units, which dynamically regulate the band structures and optoelectronic properties of hybrid halides.[15-16] Interestingly, some OIMHs also directly exhibit the characteristic emissions mainly originating from the organic cations.[17-18]On the other hand, the inorganic skeletons directly contribute to the band structures and help determine the excited state energy and PL properties. Hence, the diversified organic cations and variegated inorganic halide skeletons afford multiple design strategies to tune the PL properties of hybrid halides.

To date, many OIMHs with 0D structure have been reported as efficient emitters, such as $(C_9NH_{20})_2SnBr_4$,[15] $(C_9NH_{20})_7(PbCl_4)Pb_3Cl_{11}{\cdot}CH_3CN$,[19] $(C_5H_7N_2)_2MBr_4$ (*M* = Hg and Zn),[20] $(C_8NH_{12})_4Bi_{0.57}Sb_{0.43}Br_7{\cdot}H_2O$[21] and (18-crown-6)$_2Na_2(H_2O)_3Cu_4I_6$[22]. However, the currently reported highest efficiency 0D materials are mostly based on Pb, Sn or Sb, and the toxicity of Pb and the ease of oxidation of Sn and Cu^+ limit the commercial application of 0D materials. Therefore, exploring new, stable, nontoxic, high efficiency luminescent 0D materials with Sb^{3+} or Bi^{3+} is a key challenge to be addressed. In our work, we used N, N, N′·trimethylethylenediamine (TMEDA) and Bi or Sb halides to synthesize 0D metal halides to unveil the relationship between crystal structure and PL efficiency.

Herein, a series of zero-dimensional OIMHs were prepared, namely, $(TMEDA)_3Bi_2Cl_{12}{\cdot}H_2O$ **(1)**, $(TMEDA)_3Bi_2Br_{12}{\cdot}H_2O$ **(2)**, $(TMEDA)_5Sb_6Cl_{28}{\cdot}2H_2O$ **(3),** and $(TMEDA)_3Sb_2Br_{12}{\cdot}H_2O$ **(4)**. Compounds **1**, **2**, and **4** are isostructural, crystallizing in the monoclinic space group, and compound **3** crystallizes in the orthorhombic space group. Through UV–vis optical absorption spectra measurements of the obtained powders, we determined the optical band gaps to be 3.37 eV, 2.95 eV, 3.56 eV and 2.88 eV for compounds 1–4, respectively. Density functional theory (DFT) calculation was performed to determine the compositions of the bands. The PL intensities of the four compounds were measured and compared to unveil the origin of the strong PL of compound **3**.

2. Experimental section

Reagents. TMEDA with a purity of 97% was obtained from HWRK CHEM. $BiCl_3$ (99.9%), $BiBr_3$ (99.9%), $SbCl_3$ (99.9%), and $SbBr_3$ (99.9%) were purchased from Aladdin Company. HCl (36–38 wt.% in H_2O) and HBr (48 wt.% in H_2O) were obtained from Beijing Chemical Works.

Synthesis. For the synthesis of **1,** a mixture of $C_5H_{14}N_2$ (260 µL) and $BiCl_3$ (0.628 g) was dissolved in 2 mL of HCl under heating and continuous stirring at ~70 °C until the solution becomes clear, then slowly cooled (1.0 °C /h) to room temperature. Finally, colorless crystals were obtained. The yield of the reaction based on Bi element was ~62%. Compound **2** was obtained by the same method with the starting material of $C_5H_{14}N_2$ (130 µL) and $BiBr_3$ (0.449 g) dissolved in 4 mL of HBr. Finally, large bulk light-yellow crystals were obtained. The yield of the reaction based on Bi element was ~70%. For compound **3** a mixture of $C_5H_{14}N_2$ (130 µL) and $SbBr_3$ (0.362 g) was dissolved in 5 mL of HBr and similar method was used as compound **1**. Finally, large bulk light-yellow crystals were obtained. The yield of the reaction based on Sb element was ~66%. The synthesis of **4** was also similar, and a mixture of $C_5H_{14}N_2$ (260 µL) and $SbBr_3$ (0.685 g) was dissolved in 3 mL of HBr. Finally, white crystals were obtained. The yield of the reaction based on Sb element was ~63%.

Characterization. Single-crystal X-ray diffraction (SCXRD) analysis was performed for crystals of **2** and **3**. Data collection was performed with Mo Kα radiation using Rigaku XtaLAB PRO. Using the SHELXTL package, crystal structures were solved and refined.[23] Powder X-ray diffraction (PXRD) patterns were obtained using a D8 Advance diffractometer (Bruker Corporation, Germany) operating at 40 kV and 40 mA with Cu Kα radiation. Scanning electron microscopy (SEM) and energy-dispersive X-ray spectroscopy (EDS) analyses were performed using a JEOL JSM·6510 scanning electron microscope. Absorption spectra were obtained using a SHIMADZU UV·3600 with the grounded powders. A FLSP9200 from Edinburgh Instruments Ltd., UK was used to analyze the steady-state PL spectra, and luminescence decay curves of the powders were obtained using a Shimadzu UV·3600. The powders (~20 mg) were used for thermogravimetric analysis (TGA) using a Setaram Labsys Evo at the heating and cooling rate of ± 10 °C/min.

DFT calculation. DFT calculation was performed using periodic boundary conditions and a plane-wave basis set as implemented in the Vienna ab initio simulation package.[24] Using a basis set energy cutoff of 500 eV the calculations of DFT were converged to ~ 3 meV/cation and in the Brillouin zone dense k-meshes corresponding to 4000 k-points for per reciprocal atom.

3. Results and Discussion

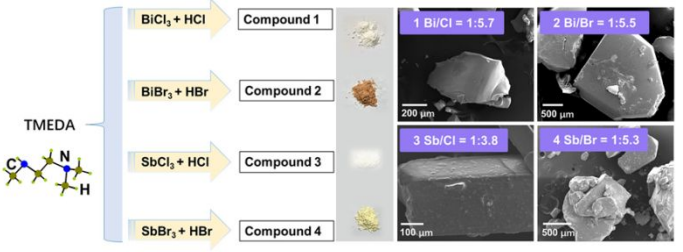

Figure 1. (a) Diagram of reaction process of 0D compounds $(TMEDA)_3Bi_2Cl_{12}{\cdot}H_2O$ **(1)**, $(TMEDA)_3Bi_2Br_{12}{\cdot}H_2O$ **(2)**, $(TMEDA)_5Sb_6Cl_{28}{\cdot}2H_2O$ **(3),** and $(TMEDA)_3Sb_2Br_{12}{\cdot}H_2O$ **(4). (b)** SEM images of compounds **1–4**.

Synthetic Methods and Crystal Structure. The title compounds were prepared by dissolving the starting materials of metal

halides and TMEDA into HCl (HBr) at ~70 °C, followed by slowly cooling to room temperature (Figure 1). High-quality single crystals were obtained. SEM images and EDS analysis of the title compounds indicated that the elemental ratio of metal to halides in compounds **1–4** was approximately 1:5.67, 1:5.46, 1:3.83, and 1:5.33, respectively. These values are almost identical to the crystallographic analysis results.

The structures of **2** and **3**·were determined by SCXRD. The PXRD measurements revealed that compounds **1**, **2**, and **4** are isostructural; thus, the structures of **1** and **4** were refined using **2** as the starting structure model using the Rietveld method (Figure 2). Compounds **1**, **2**, and **4** crystallize in the monoclinic space group $P2_1/n$, and compound **3** crystallizes in the orthorhombic space group *Pnma*. The unit cell parameters and crystal structural refinement details of **2** and **3** are shown in Table 1, and the more details of the obtained strucutres are listed inTable S1–S8.

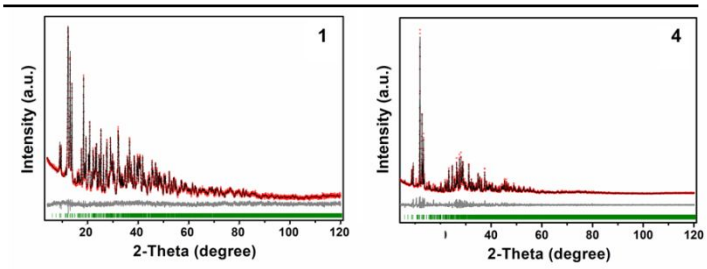

Figure 2. Powder X-ray diffraction and Rietveld refinement of (a) $(TMEDA)_3Bi_2Cl_{12}·H_2O$ **(1)** and (b) $(TMEDA)_3Sb_2Br_{12}·H_2O$ **(4)**

Table 1. Crystal data and structure refinement for compounds **2** and **3** at 293 (2) K.

Compound	**2**	**3**
Empirical formula	$C_{15}H_{48}Bi_2Br_{12}N_6O$	$C_{25}H_{80}Cl_{28}N_{10}O_2Sb_6$
Formula weight	1707.49	2270.04
Temperature	293(2) K	293(2) K
Wavelength	0.71073 Å	0.71069 Å
Crystal system	monoclinic	orthorhombic
Space group	$P2_1/n$	*Pnma*
Unit cell dimensions	a = 10.4313(3) Å,	
	b = 13.2804(5) Å,	a = 24.279 Å,
	c = 29.8495(9) Å,	b = 31.441 Å,
	β = 95.670(3)°	c = 10.132 Å
Volume	4114.9(2) Å^3	7734.1 Å^3
Z	4	4
Density (calculated)	2.756 g/cm^3	1.950 g/cm^3
Absorption coefficient	20.215 mm^{-1}	3.067 mm^{-1}
F(000)	3104	4368
ϑ range for data collection	2.57° to 25.00°	2.70° to 26.37°
Index ranges	-12<=h<=12, -15<=k<=15, -35<=l<=35	-29<=h<=30, -39<=k<=38, -12<=l<=12
Reflections collected	33865	48597

Independent reflections	7235 [R_{int} = 0.0541]	8054 [R_{int} = 0.0582]
Completeness to ϑ =25.00°	99.8%	99.8%
Refinement method	Full-matrix least-squares on F^2	
Data / restraints / parameters	7235 / 2 / 342	8054 / 0 / 331
Goodness-of-fit	1.020	1.068
Final R indices [$I > 2\sigma(I)$]	R_{obs} = 0.0310, w_{Robs} = 0.0642	R_{obs} = 0.0318, w_{Robs} = 0.0724
R indices [all data]	R_{all} = 0.0417, w_{Rall} = 0.0669	R_{all} = 0.0416, w_{Rall} = 0.0758
Largest diff. peak and hole	1.325 and -1.461 e·Å^{-3}	1.309 and -1.089 e·Å^{-3}

$R = \Sigma||F_o|-|F_c|| / \Sigma|F_o|$, $wR = \{\Sigma[w(|F_o|^2 - |F_c|^2)^2] / \Sigma[w(|F_o|^4)]\}^{1/2}$ and $w = 1/[\sigma^2(F_o^2)+(0.0462P)^2]$ where $P=(F_o^2+2F_c^2)/3$

As shown in Figure 3, all of the compounds have a 0D structure, and each Bi/Sb is coordinated with six adjacent Cl/Br atoms, forming distorted octahedra. Because compounds **1**, **2**, **4** are isostructural, only the structure of **2** will be discussed in detail. Compound **2** consists of isolated octahedra separated by organic cations $C_7H_{10}N^{2+}$. Compound **3** consists of a combination of corner-connected octahedra dimers $[Sb_2Cl_{10}]^{4-}$ and $[Sb_4Cl_{18}]^{6-}$ clusters with edge- and corner-sharing octahedra. The corner-connected octahedra are inclined to form higher-dimensional frameworks (3D, 2D, 1D), whereas corner-connected 0D OIMHs are quite rare with only seven compounds known to contain corner-sharing dimeric $[M_2X_{11}]^{5-}$ anions.[25] Instead, 0D octahedral clusters tend to form edge-sharing or face-sharing octahedra to help reduce the total charge of the anion.[26]

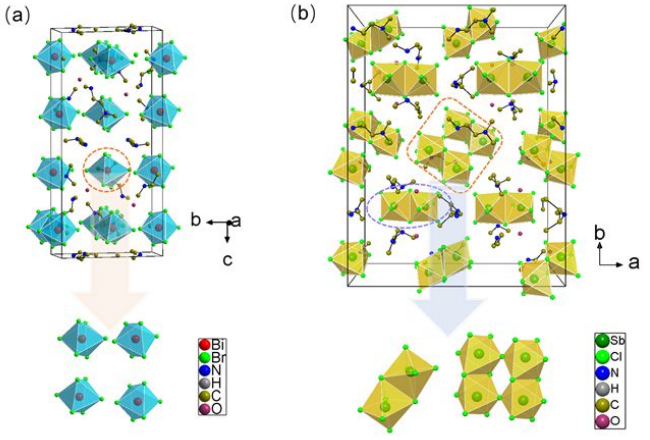

Figure 3. Crystal structures and the inorganic moieties of 0D OIMHs (a) $(TMEDA)_3Bi_2Br_{12}·H_2O$ **(2)** and (b) $(TMEDA)_5Sb_6Cl_{28}·2H_2O$ **(3)**.

The metal–halide interatomic distances within the series of $[MX_6]^{3-}$ (M = Bi^{3+}, Sb^{3+}; X = Cl^-, Br^-) contract following the shrinking of the ionic radii moving from bromine to chlorine. The bond lengths of $[BiX_6]^{3-}$ range from 2.7672(7) to 2.9353(6) Å for **2** and from 2.671(13) to 2.807(15) Å for **1**. These bond lengths are in the same range as those of reported compounds with similar structures $(C_7H_{10}N)BiBr_6·H_2O$ (2.892–2.941 Å) and $(C_4H_{16}N_3)BiBr_6$ (2.829–2.8643 Å).[27-28] The Cl–Bi–Cl bond angles are 80.98(46)° for **1**， and **2** has smaller distortion angles with bond angles ranging from 83.786(19) to 97.43(2)°. The deviation of these values from 90° indicates that the inorganic octahedra are distorted. The distorted nature of the octahedra could be due to slight or dynamic stereochemical activity of a lone pair on the Bi^{3+} center, as previously observed in other bismuth or tin halide compounds.[29-31] In compounds **3** and **4**, the Sb–X bond length is slightly shorter than the Bi–X bond length, which is consistent with the Shannon radii of 1.03 Å for Bi and 0.76 Å for Sb in six coordination environments.[32] The antimony-based compounds have significantly more distorted octahedra, with the bond lengths of $[SbX_6]^{3-}$ range from 2.4101(11) to 2.8775(11) for **3** and from 2.622(19) to 3.113(18) for 4. This further implicates the role of lone-pair stereo activity, which is expected to strengthen when the metal s and ligand p orbitals become closer in energy,[33-34] as the same trends were observed in $CsMX_3$-based compounds, where M spans from Ge, Sn, and Pb and X is a halogen.[35-38] In fact, the longest Sb–Cl bond lengths (3.082 Å) and Sb–Br bond lengths (3.163 Å) are longer than the longest Bi–Cl and Bi–Br lengths (2.807 and 2.935 Å, respectively), highlighting the large degree of octahedral distortion in the Sb compounds. To evaluate the octahedral distortion, the following equations were used:[39]

$$\lambda_{oct} = \frac{1}{6}\sum_{n=1}^{6}[(d_n - d_0)/d_0]^2$$

$$\sigma^2 = \frac{1}{11}\sum_{n=1}^{12}(\theta_n - 90^\circ)^2$$

where d_n are the M–X bond lengths, d_0 is the average M–X bond distance, and θ_i are the angles of M–X–M. The avergy distance and

angle distortion of **1, 2**, **3** are less than that of **4** (Table 2), which indicates that **4** may have a better PL property at room temperature.

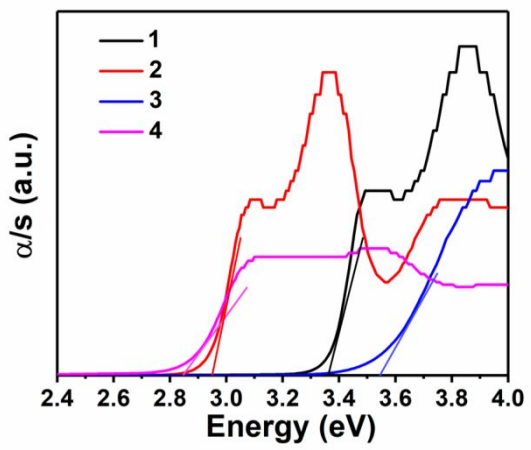

Figure 4. Optical absorption spectra of compounds $(TMEDA)_3Bi_2Cl_{12}\cdot H_2O$ **(1)**, $(TMEDA)_3Bi_2Br_{12}\cdot H_2O$ **(2)**, $(TMEDA)_5Sb_6Cl_{28}\cdot 2H_2O$ **(3),** and $(TMEDA)_3Sb_2Br_{12}\cdot H_2O$ **(4)**.

Stability, Optical Properties and DFT Calculations. Thermal stability of compounds **1–4** was explored, TGA was conducted under a nitrogen atmosphere **(**Figure S1**)**. It is apparent from the TGA curves that **2** is most stable and loses weight until 250 °C. **1** and **4** exhibit poorer thermal stability (stable up to 200 °C). The difference is that when the temperature rises to 600 °C, **4** completely decomposes, whereas for **1**, only 60% of the initial weight is lost. **3** shows the worst stability (stable below 150 °C) and loses most of its mass at 260 °C. This is because the corner-connected octahedra $[Sb_4Cl_{18}]^{6-}$ and edge-shared $[Sb_2Cl_{10}]^{4-}$ are very unstable and easy to decompose at elevated temperature.

Through UV–vis optical absorption spectra measurements of the obtained powders, we determined the optical band gaps to be 3.37 eV, 2.95 eV, 3.56 eV and 2.88 eV for compounds **1–4**, respectively, by extrapolating the linear portion of the absorption edges (Figure 4). The spectra reveal significant absorption of visible light with relatively sharp edges for all the compounds. The absorption edges for compounds **2** and **4** are all red shifted relative to those for **1** and **3**. To obtain further insight on the optical absorption, theoretical studies on compounds **1–4** were performed using DFT calculations. The calculated band gaps of compounds **1–4** were 3.98, 2.30, 3.14, and 2.23 eV, respectively (Figure S2). As shown in Figure S3, for compounds **1** and **3**, the valence band maximum (VBM) consists of Bi 6s and Br 4p (Cl 3p) states at *H*, and the conduction band minimum (CBM) consists mainly of the Bi 6p state at *X*. Similarly, the VBM of **2** and **4** mainly consists of Sb 5s and Br 4p (Cl 3p) states at *H*, and the CBM consists mainly of the Sb 5p state at *X*. The valence band is composed of primarily *X* (*X* = Cl, Br) p orbitals with a vanishingly small contribution from the Sb s orbitals and Bi s orbitals at the band edge. For these 0D materials, the dispersion of their valence band and conduction band is very small, indicating that their electronic states are very local. Therefore, the inorganic octahedra can be also regarded as isolated luminescence centers, and the PL can be discussed in terms of electronic transition among the molecular orbital energy levels.

Table 2. Summary of important photophysical parameters of compounds **1-4**.

compound	Band gap (eV)	λ_{ex} (nm)	λ_{em} (nm)	Stokes shift (nm)	FWHM (nm)	average λ_{oct} (×10^{-2})	average σ^2 (deg.^{2})	PLQY
1	3.98	290	460	170	207	1.155	27.73	<1%
2	2.30	254	405	151	48	1.605	13.695	<1%
3	3.14	400	600	200	253	9.065	9.287	<1%
4	2.33	400	625	225	150	6.73	29.675	10%

In Table 2, compounds **1**, **2,** and **3** show weak photoluminescence in at room temperature, the specific optical properties are shown in Figure S4, whereas **4** exhibited good luminescence properties. This finding further confirmed that the light emission of low-dimensional halides based on the $5s^2$ cations Sb^{3+} are stronger than that based on the $6s^2$ cations Bi^{3+}, and the structures with isolated octahedra were more likely to produce intense PL emission.[11, 40] Figure 5a presents the normalized PL emission spectra of $(TMEDA)_3Sb_2Br_{12}\cdot H_2O$. Upon 400 nm excitation, broadband yellow emission centered at 625 nm with a large Stokes shift of 225 nm was observed at RT. The PL band ranges from 450 to 800 nm with a full-width at half-maximum (FWHM) of ~150 nm. Such broad emission is commonly observed in low-dimensional OIMHs, which is attributed to STE emission.[21, 41-42] Figure 5b presents typical luminescence decay curves of **4** monitored at 620 nm emission at RT. The curve can be fitted by a single exponential function with average luminescence lifetime of 34.7 ns with an excitation wavelength of 400 nm. The short decay time may be related to spin-triplet excited states transitions of $^3P_1 \rightarrow {}^1S_0$.[43-44] Furthermore, the emission curve under the excitation of different wavelengths was exactly the same as that obtained under 365-nm excitation, indicating that **4** exists only one emission center (Figure 5c). Compound **4** shows CIE chromaticity coordinates of (0.5421, 0.4460) in the color gamut, consistent with the yellow PL (Figure 5d).

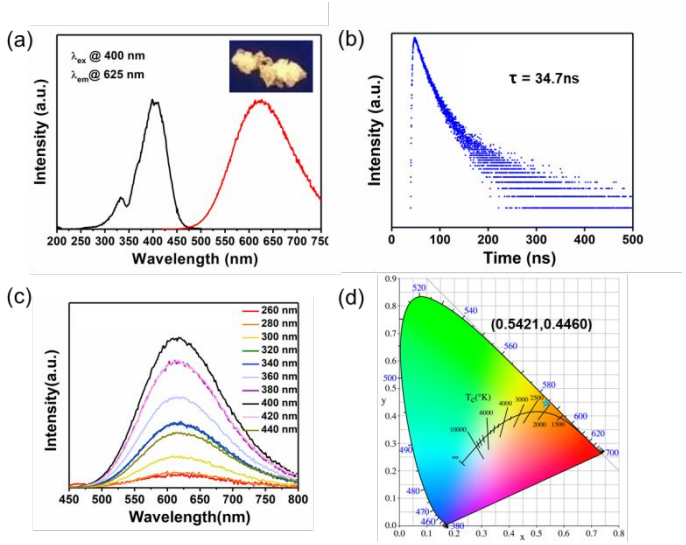

Figure 5. (a) PLE and PL spectra of $(TMEDA)_3Sb_2Br_{12}·H_2O$ **(4)** at RT. (b) PL decay curves of **4** polycrystalline powder upon 400-nm excitation monitored at 625 nm at RT. (c) The PL of **4** under different excitation wavelengths. (d) CIE color coordinates of **4**.

To probe the mechanism of the broad emission, we performed temperature-variable PL spectroscopy analysis of **4** with the excitation wavelength of 400 nm. The temperature-dependent PL spectra for $(TMEDA)_3Sb_2Br_{12}·H_2O$ from 80 to 380 K are presented in Figure 6a. With increasing temperature, the intensity of the emission peak decreases monotonically owing to the increase of non-radiative recombination,[45] and the width of the FWHM increases, which can be described by the following law:[46]

$$\mathrm{f(T)} = 2.36 \times \sqrt{S} \times E_{ph} \times \left[\coth\left(\frac{E_{ph}}{2kT}\right)\right]^{1/2},$$

where $\mathrm{f(T)}$ is the FWHM at different temperatures, S is the Huang–Rhys parameter, *k* is the Boltzmann constant, and E_{ph} is the effective phonon energy. As is shown in Figure S5, we can calculate that compound **4** has S = 21.2 and E_{ph} = 28.3 meV, which at the same lever of reported hybrid metal halides, i. e. $C_5N_2H_{16}PbBr_6$.[47] The *S* values of compound **4** is greater than the reported inorganic compounds, such as 8.4 for $Y_3Al_5O_{12}$,[48] and 9.0 for $Lu_3Al_5O_{12}$, implying that strong electron–phonon coupling in compound **4**. Furthermore, the values of E_{ph} is larger than the fully-inorganic metal halides, such as $Cs_3Bi_2I_6Cl_3$ (E_{ph} = 4.0 meV)[49] and $Cs_2AgInCl_6$ (E_{ph} = 17.4 meV),[50] indicating that **4** lattice vibrational energy is relatively large and with relatively weak structural rigidity.

The "static" lone pair is expressed and found in coordinatively unsaturated geometries such as disphenoids (SnX_4) and square pyramids (SbX_5). In both cases, the reduced symmetry imposed by these motifs results in nondegenerate excited states, which may allow for additional transitions if the energy levels are sufficiently separated, although the separation may be quite small.[51] This has been demonstrated by Morad et al., with the observation of both $^3P_1 \rightarrow {}^1S_0$ and $^1P_1 \rightarrow {}^1S_0$ transitions at RT in disphenoidal $(Bmpip)_2SnBr_4$ (Bmpip is 1-butyl-1-methylpiperidinium cation).[52] This situation is simplified in octahedrally coordinated systems (Figure 6b). The larger coordination number reduces the static expression of the lone pair and therefore off-centering and distortion, leading to high-symmetry sites and similar bond lengths. The regularity (or near-regularity) of such sites obscures the optical properties present in the disphenoidal and different metal centers and different degrees of distortion or lone-pair expression, the PL spectra appear to be triplet ($^3P_{0,1,2}$) dominated with one broad, featureless emission peak. This can be understood in terms of the higher degeneracy of the regular octahedral environment; whereas the trigonally distorted octahedron would have fully distinct singlet and triplet states, the regular octahedron does not fully separate these levels, and therefore, the singlet remains unobserved.[51]

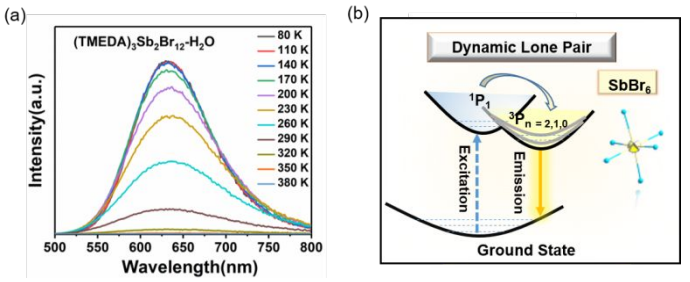

Figure 6. (a) Temperature-dependent (80 to 380 K) PL spectra of $(TMEDA)_3Sb_2Br_{12}·H_2O$ **(4)**. (b) Schematic illustration of luminescence mechanism of **4**.

4. Conclusions

We report a new family of compounds $(TMEDA)_3Bi_2Cl_{12}·H_2O$ **(1)**, $(TMEDA)_3Bi_2Br_{12}·H_2O$ **(2)**, $(TMEDA)_5Sb_6Cl_{28}·2H_2O$ **(3),** and $(TMEDA)_3Sb_2Br_{12}·H_2O$ **(4)**. Compounds **1**, **2**, and **4** are isostructural with a 0D structure consisting of individual metal halide ions ($[BiCl_6]^{3-}$, $[BiBr_6]^{3-}$ and $[SbBr_6]^{3-}$) that are completely isolated from each other by large organic cations. Compound **3** consists of a combination of corner-connected octahedral dimers $[Sb_2Cl_{10}]^4$ and corner-, edge-sharing octahedral $[Sb_4Cl_{18}]^{6-}$ clusters. All the compounds are ambient stable with semiconducting properties. Among these compounds, **4** shows the most intense PL at room temperature. The optical bandgap of **4** was experimentally determined to be 2.88 eV. Upon 400 nm light excitation, **4** exhibited strong broadband orange luminescence with a FWHM of ~150 nm resulting from self-trapped exciton emission. The efficient PL of 4 was shown to be related to the lone-pair-containing $5s^2$ Sb^{3+} cation, which possess suitable electric bands that are conducive to visible-light emission. By comparing the PL intensities of metal halides with different metal centers and structures, this work serves

as a case study of the relationship between structure and photoluminescence properties, which may promote further applications in WLEDs and the design of phosphors.

Supporting Information

Atomic coordinates and equivalent isotropic displacement parameters, bond lengths, TGA curves, band structures, densities of states and orbital projections, PLE and PL spectra, fitting of the FWHM.

Corresponding Author

* jingzhao@ustb.edu.cn

* qlliu@ustb.edu.cn

Conflicts of interest

The authors declare no competing financial interest.

Acknowledgements

This work was supported by Beijing Municipal Natural Science Foundation (2182080) and the National Natural Science Foundation of China (51972021 and 51702329). The work was partly supported by the Fundamental Research Funds for the Central Universities (FRF-IDRY-19-005) and by the RFBR according to the research project No.19-52-80003. S.H. and C.W. (DFT calculations) acknowledge support from the Department of Energy, Office of Science Basic Energy Sciences under Grant DE-SC0014520. Access to QUEST, the supercomputing resources facilities at Northwestern University, is also acknowledged.

Notes and references

1. M. Ahmadi, T. Wu and B. Hu, *Adv. Mater.*, 2017, **29**, 1605242.
2. H. Tsai, W. Nie, J. C. Blancon, C. C. Stoumpos, R. Asadpour, B. Harutyunyan, A. J. Neukirch, R. Verduzco, J. J. Crochet, S. Tretiak, L. Pedesseau, J. Even, M. A. Alam, G. Gupta, J. Lou, P. M. Ajayan, M. J. Bedzyk and M. G. Kanatzidis, *Nature*, 2016, **536**, 312-316.
3. L. Mao, W. Ke, L. Pedesseau, Y. Wu, C. Katan, J. Even, M. R. Wasielewski, C. C. Stoumpos and M. G. Kanatzidis, *J. Am. Chem. Soc.*, 2018, **140**, 3775-3783.
4. Z. K. Tan, R. S. Moghaddam, M. L. Lai, P. Docampo, R. Higler, F. Deschler, M. Price, A. Sadhanala, L. M. Pazos, D. Credgington, F. Hanusch, T. Bein, H. J. Snaith and R. H. Friend, *Nat. Nanotechnol.*, 2014, **9**, 687-692.
5. P. Y. Gu, N. Wang, C. Wang, Y. Zhou, G. Long, M. Tian, W. Chen, X. W. Sun, M. G. Kanatzidis and Q. Zhang, *J. Mater. Chem. A*, 2017, **5**, 7339-7344.
6. R. Gautier, F. Massuyeau, G. Galnon and M. Paris, *Adv. Mater.*, 2019, **31**, e1807383.
7. Z. Song, J. Zhao and Q. Liu, *Inorg. Chem. Front.*, 2019, **6**, 2969-3011.
8. W. S. Yang, B. W. Park, E. H. Jung, N. J. Jeon, Y. C. Kim, D. U. Lee, S. S. Shin, J. Seo, E. K. Kim, J. H. Noh and S. I. Seok, *Science*, 2017, **356**, 1376-1379.
9. M. Yuan, L. N. Quan, R. Comin, G. Walters, R. Sabatini, O. Voznyy, S. Hoogland, Y. Zhao, E. M. Beauregard, P. Kanjanaboos, Z. Lu, D. H. Kim and E. H. Sargent, *Nat. Nanotechnol.*, 2016, **11**, 872-877.
10. B. Saparov and D. B. Mitzi, *Chem. Rev.*, 2016, **116**, 4558-4596.
11. V. Morad, S. Yakunin, B. M. Benin, Y. Shynkarenko, M. J. Grotevent, I. Shorubalko, S. C. Boehme and M. V. Kovalenko, *Adv. Mater.*, 2021, **33**, e2007355.
12. R. Gautier, R. Clerac, M. Paris and F. Massuyeau, *Chem. Commun. (Camb.)*, 2020, **56**, 10139-10142.
13. M. I. Saidaminov, J. Almutlaq, S. Sarmah, I. Dursun, A. A. Zhumekenov, R. Begum, J. Pan, N. Cho, O. F. Mohammed and O. M. Bakr, *ACS Energy Lett.*, 2016, **1**, 840-845.
14. M. Li and Z. Xia, *Chem. Soc. Rev.*, 2021, **50**, 2626-2662.
15. C. Zhou, H. Lin, H. Shi, Y. Tian, C. Pak, M. Shatruk, Y. Zhou, P. Djurovich, M. H. Du and B. Ma, *Angew. Chem. Int. Ed. Engl.*, 2018, **57**, 1021-1024.
16. L. Lanzetta, J. M. Marin-Beloqui, I. Sanchez-Molina, D. Ding and S. A. Haque, *ACS Energy Lett.*, 2017, **2**, 1662-1668.
17. A. Yangui, S. Pillet, E.-E. Bendeif, A. Lusson, S. Triki, Y. Abid and K. Boukheddaden, *ACS Photonics*, 2018, **5**, 1599-1611.
18. R. Roccanova, M. Houck, A. Yangui, D. Han, H. Shi, Y. Wu, D. T. Glatzhofer, D. R. Powell, S. Chen, H. Fourati, A. Lusson, K. Boukheddaden, M. H. Du and B. Saparov, *ACS Omega*, 2018, **3**, 18791-18802.
19. C. Zhou, H. Lin, M. Worku, J. Neu, Y. Zhou, Y. Tian, S. Lee, P. Djurovich, T. Siegrist and B. Ma, *J. Am. Chem. Soc.*, 2018, **140**, 13181-13184.

20. A. Yangui, R. Roccanova, T. M. McWhorter, Y. Wu, M.-H. Du and B. Saparov, *Chem. Mater.*, 2019, **31**, 2983-2991.
21. R. Zhang, X. Mao, Y. Yang, S. Yang, W. Zhao, T. Wumaier, D. Wei, W. Deng and K. Han, *Angew. Chem. Int. Ed. Engl.*, 2019, **58**, 2725-2729.
22. J. Huang, B. Su, E. Song, M. S. Molokeev and Z. Xia, *Chem. Mater.*, 2021, **33**, 4382-4389.
23. G. M. Sheldrick, *Acta Crystallogr. A*, 2008, **64**, 112-122.
24. G. Kresse and J. Furthmuller, *Phys. Rev. B Condens. Matter.*, 1996, **54**, 11169-11186.
25. R. Jakubas, M. Rok, K. Mencel, G. Bator and A. Piecha-Bisiorek, *Inorg. Chem. Front.*, 2020, **7**, 2107-2128.
26. K. M. McCall, V. Morad, B. M. Benin and M. V. Kovalenko, *ACS Mater. Lett.*, 2020, **2**, 1218-1232.
27. D. Chen, F. Dai, S. Hao, G. Zhou, Q. Liu, C. Wolverton, J. Zhao and Z. Xia, *J. Mater. Chem. C*, 2020, **8**, 7322-7329.
28. H. Dammak, H. Feki, H. Boughzala and Y. Abid, *Spectrochim. Acta. A Mol. Biomol. Spectrosc.*, 2015, **137**, 1235-1243.
29. D. H. Fabini, G. Laurita, J. S. Bechtel, C. C. Stoumpos, H. A. Evans, A. G. Kontos, Y. S. Raptis, P. Falaras, A. Van der Ven, M. G. Kanatzidis and R. Seshadri, *J. Am. Chem. Soc.*, 2016, **138**, 11820-11832.
30. K. K. Bass, L. Estergreen, C. N. Savory, J. Buckeridge, D. O. Scanlon, P. I. Djurovich, S. E. Bradforth, M. E. Thompson and B. C. Melot, *Inorg. Chem.*, 2017, **56**, 42-45.
31. S. Sun, S. Tominaka, J.-H. Lee, F. Xie, P. D. Bristowe and A. K. Cheetham, *APL Mater.*, 2016, **4**.
32. R. D. Shannon, *Acta Crystallogr. A*, 1976, **32**, 751-767.
33. A. Walsh, D. J. Payne, R. G. Egdell and G. W. Watson, *Chem. Soc. Rev.*, 2011, **40**, 4455-4463.
34. U. V. Waghmare, N. A. Spaldin, H. C. Kandpal and R. Seshadri, *Phys. Rev. B*, 2003, **67**.
35. G. Laurita, D. H. Fabini, C. C. Stoumpos, M. G. Kanatzidis and R. Seshadri, *Chem. Sci.*, 2017, **8**, 5628-5635.
36. C. C. Stoumpos, L. Frazer, D. J. Clark, Y. S. Kim, S. H. Rhim, A. J. Freeman, J. B. Ketterson, J. I. Jang and M. G. Kanatzidis, *J. Am. Chem. Soc.*, 2015, **137**, 6804-6819.
37. F. Hao, C. C. Stoumpos, R. P. Chang and M. G. Kanatzidis, *J. Am. Chem. Soc.*, 2014, **136**, 8094-8099.
38. C. C. Stoumpos, C. D. Malliakas and M. G. Kanatzidis, *Inorg. Chem.*, 2013, **52**, 9019-9038.
39. K. Robinson, G. V. Gibbs and P. H. Ribbe, *Science*, 1971, **172**, 567-570.
40. B. Su, M. Li, E. Song and Z. Xia, *Adv. Funct. Mater.*, 2021, DOI: 10.1002/adfm.202105316, 2105316.
41. M. D. Smith and H. I. Karunadasa, *Acc. Chem. Res.*, 2018, **51**, 619-627.
42. Y. Jing, Y. Liu, M. Li and Z. Xia, *Adv. Opt. Mater.*, 2021, **9**, 2002213.
43. Kang, F. Zhang, H. Wondraczek, L. Yang, X. Zhang, Y. Lei, D. Y. Peng, M, *Chem Mater*., 2016, **28**, 2692-2703.
44. Jing, Y. Liu, Y. Jiang, X. Molokeev, M. S. Lin, Z. Xia, Z., *Chem Mater*., 2020, **32**, 5327-5334.
45. R. Gautier, M. Paris and F. Massuyeau, *J. Am. Chem. Soc.*, 2019, **141**, 12619-12623.
46. J. Lee, E. S. Koteles and M. O. Vassell, *Phys. Rev. B Condens. Matter.*, 1986, **33**, 5512-5516.
47. H. Luo, S. Guo, Y. Zhang, K. Bu, H. Lin, Y. Wang, Y. Yin, D. Zhang, S. Jin, W. Zhang, W. Yang, B. Ma and X. Lu, *Adv. Sci. (Weinh)*, 2021, **8**, e2100786.
48. V. Bachmann, C. Ronda and A. Meijerink, *Chem. Mater.*, 2009, **21**, 2077-2084.
49. K. M. McCall, C. C. Stoumpos, O. Y. Kontsevoi, G. C. B. Alexander, B. W. Wessels and M. G. Kanatzidis, *Chem. Mater.*, 2019, **31**, 2644-2650.
50. J. Luo, X. Wang, S. Li, J. Liu, Y. Guo, G. Niu, L. Yao, Y. Fu, L. Gao, Q. Dong, C. Zhao, M. Leng, F. Ma, W. Liang, L. Wang, S. Jin, J. Han, L. Zhang, J. Etheridge, J. Wang, Y. Yan, E. H. Sargent and J. Tang, *Nature*, 2018, **563**, 541-545.
51. A. Vogler and H. Nikol, *Comments Inorg. Chem.*, 1993, **14**, 245-261.
52. V. Morad, Y. Shynkarenko, S. Yakunin, A. Brumberg, R. D. Schaller and M. V. Kovalenko, *J. Am. Chem. Soc.*, 2019, **141**, 9764-9768.

